for the sequence of specific heat exponents $\alpha^{(\nu)}$. The reason is of course that the "critical indices" (such as $\alpha^{(\nu)}$) are defined as the $T\to T_c$ limit of certain functionals $f[\psi^{(\nu)}(T)]$, and we cannot rule out the possibility that

$$\lim_{\nu\to\infty}\{\lim_{T\to T_c} f[\psi^{(\nu)}(T)]\} \neq \lim_{T\to T_c} f[\psi^{\mathrm{SM}}(T)]. \quad \text{(A3)}$$

Although the terms in the various high-temperature expansions would have to depart from their apparently smooth variation with ν at *some* order if the critical indices were to behave discontinuously as a function of ν, the fact that there is absolutely no indication of this through order $1/T^{10}$ does not *prove* anything one way or the other.

PHYSICAL REVIEW VOLUME 176, NUMBER 2 10 DECEMBER 1968

Magnetic Structures of Er_2O_3 and Yb_2O_3†

R. M. Moon, W. C. Koehler, H. R. Child, and L. J. Raubenheimer*
Solid State Division, Oak Ridge National Laboratory, Oak Ridge, Tennessee
(Received 21 June 1968)

The magnetic structures of Er_2O_3 and Yb_2O_3 have been determined by analysis of neutron diffraction data on powders and single crystals. Noncollinear antiferromagnetic structures were found, with the moment direction related to the local symmetry axis. For Er_2O_3, the moment on the C_2 site is $(5.36\pm0.08)\mu_B$ and at the C_{3i} site the moment is $(6.06\pm0.23)\mu_B$. For Yb_2O_3, the corresponding moments are $(1.86\pm0.06)\mu_B$ and $(1.05\pm0.06)\mu_B$. The Néel points are 3.4°K for Er_2O_3 and 2.3°K for Yb_2O_3. Calculations of the dipole-dipole energies for the observed structures indicate that the dipole forces are not sufficient to explain the structures. The dependence of the long-range magnetic order on the reduced temperature is the same in both systems. Good agreement with this temperature dependence was obtained by assuming a biquadratic exchange interaction and making a simple molecular-field approximation.

I. INTRODUCTION

THE rare-earth oxides form an interesting class of magnetic materials because of their weak magnetic interactions. For example, the Néel points of Er_2O_3 and Yb_2O_3 are 3.4 and 2.3°K, respectively. These temperatures are low enough that the magnetic dipole interaction must be considered a possible cause of the magnetic order. One of the objectives of this investigation was to evaluate the importance of the dipole interaction by deducing the magnetic structure from neutron diffraction data, calculating the dipolar interaction energy of this structure, and comparing the result with the observed Néel temperature. Another implication of a low Néel point is that the magnetic interaction, whatever its origin, is a small perturbation compared to the crystal-field interaction. The low-temperature magnetic properties, therefore, should be strongly influenced by the crystal field. If the magnetic interaction is very weak compared to the energy of the first excited crystal-field level, the ordered moment should be a property of the crystal-field ground state. A somewhat stronger magnetic interaction will mix the crystal-field states, as discussed by Bleaney,[1] leading to a new ground state with a moment that is a function of the strength of the magnetic interaction.

The intermediate case, in which the ground-state wave function is dependent on the strength of the magnetic interaction, can lead to unusual magnetic behavior as a function of temperature and applied field. For example, if the dominant coupling mechanism is superexchange the interatomic exchange constants are related to the rare-earth-oxygen overlap integrals. But as the degree of magnetic order increases, these overlap integrals may change because the rare-earth ground state is changing. Thus the interatomic exchange parameters are not constant, but become functions of temperature. Applied fields can also change the degree of admixture of the crystal-field states. This effect, in addition to the weak magnetic interaction, means that the magnetic structures can be easily influenced by applied fields. As an additional complication, we will see that there is some evidence indicating that biquadratic exchange may be important.

Neutron diffraction studies have been made on single crystals and powders of Er_2O_3 and Yb_2O_3. The expected complex nature of the temperature and field dependence of the magnetic structures has been fully realized.

These materials all have the bixbyite[2] structure. There are 32 rare-earth ions and 48 oxygens in a cubic unit cell with lattice constant of about 10.5 Å. The space group is $Ia3-T_h^7$. Twenty-four of the rare earths are on sites with twofold rotational symmetry (C_2), and eight are on sites with threefold rotary inversion symmetry (C_{3i}). There is one adjustable position parameter for the C_2 sites, none for the C_{3i} sites, and three for the oxygen sites. The oxygen coordination around the two rare-earth sites is shown in Fig. 1. For the C_2 site, the oxygens fall almost on the corners of a cube with the rare earth at the center and with two missing oxygens along a face diagonal. The twofold axis is perpendicular to this face diagonal. One of the symmetry elements of the space group is the body-centered translation, so that there are two C_2

† Research sponsored by the U.S. Atomic Energy Commission under contract with the Union Carbide Corporation.
* Present address: Atomic Energy Board, Pretoria Tvl., Republic of South Africa.
[1] B. Bleaney, Proc. Roy. Soc. (London) **A276, 19** (1963).
[2] L. Pauling and M. D. Shappell, Z. Kiist. **75,** 128 (1930).

sites with the configuration pictured in Fig. 1. There are six more sites with the same [100] symmetry axis but with oxygens missing along different face diagonals. Similarly there are eight sites with the twofold axis along [010] and eight along [001]. For the C_{3i} sites the missing oxygens are along ⟨111⟩ directions. There are two rare-earth sites with the local symmetry axis along each of the four different ⟨111⟩ directions. These symmetry considerations are important in visualizing the magnetic structures to be described. In general, we find noncollinear antiferromagnetic structures with the direction of the moment at each site related to the local symmetry axis.

II. EXPERIMENTAL

Single crystals of Er_2O_3 and Yb_2O_3 were obtained from K. H. Hellwege of the Technischen Hochschule, Darmstadt. These were roughly cylindrical in shape and 2–3 mm in diam. Samples were cut with flat faces parallel to the (111) plane. The crystals were immersed in liquid He in a cryostat that allowed rotation about a horizontal axis parallel to the [111] and a vertical axis perpendicular to the plane of scattering. Extensive neutron diffraction data were taken at 4.2°K, which is above the magnetic transition, and at the lowest temperature which could be reached by pumping on the He reservoir, about 1.3°K. The temperature dependence of several peaks was studied by varying the pressure over the He reservoir.

Absorption corrections were calculated using the Fortran program of Wehe, Busing, and Levy.[3] The effects of extinction and simultaneous reflections were minimized by studying crystals of different sizes. The simultaneous-reflection problem is particularly troublesome when doing diffraction measurements on crystals with large lattice spacings. The resulting high density of lattice points in reciprocal space means that there is a high probability for simultaneous reflections in any crystal orientation. For example, for a bcc lattice with $a \cong 10.5$ Å, $\lambda = 1.09$ Å, and $\delta\lambda/\lambda = 0.005$, there are an average of 57 reciprocal lattice points within the limiting spheres of reflection defined by $\delta\lambda/\lambda$. In other words, setting such a crystal on the diffractometer in a completely random orientation will result in about 57

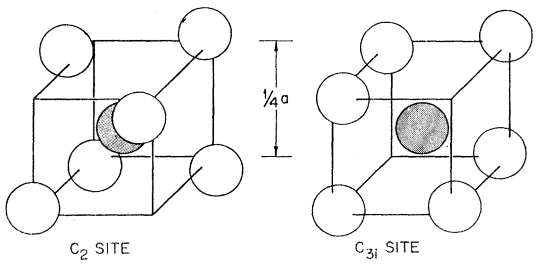

FIG. 1. Oxygen coordination around the two types of rare-earth site in the sesquioxides. Open circles are oxygen atoms.

[3] D. J. Wehe, W. R. Busing, and H. A. Levy, Oak Ridge National Laboratory Report No. ORNL-TM-229, 1962 (unpublished).

reflected beams. In this situation, it was futile to attempt to find an orientation free of simultaneous reflections by rotating about the scattering vector. Since the magnitude of the simultaneous-reflection effect depends on the crystal size,[4] as does the secondary extinction effect, these effects can be minimized by using very small crystals. The data on Er_2O_3 were collected using a crystal weighing 14 mg. For Yb_2O_3 a larger crystal (107 mg) was used because the magnetic reflections were much weaker. Questionable reflections were measured using crystals of different sizes.

The powder data were acquired in the usual way on high-purity samples of the oxides which had been fired in air just prior to being placed in the sample holders in order to drive off water and CO_2. Sample temperatures from 4.2 to ~1.3°K were reached by pumping on liquid helium in direct contact with the specimen. In a few cases, magnetic fields up to about 16 kOe were applied to the samples.

III. RESULTS—CRYSTAL STRUCTURE PARAMETERS

The measurement and analysis of nuclear intensities at 4.2°K were undertaken to provide an internal calibration for the magnetic intensities and to provide accurate positional parameters for use in the magnetic-structure analysis. This work was done at 4.2°K rather than at room temperature to avoid introducing a Debye-Waller temperature correction in the separation of nuclear and magnetic intensities. For Er_2O_3, previous work[5] had shown that some magnetic peaks were superimposed on nuclear peaks, requiring a separation by subtraction of intensities observed above and below the magnetic transition.

The single-crystal data on Er_2O_3 and Yb_2O_3 were analyzed using the least-squares program of Busing, Martin, and Levy.[6] The nuclear scattering amplitudes were taken as $b_{Er} = 0.79$, $b_{Yb} = 1.27$, and $b_0 = 0.577$ (10^{-12} cm). Lattice constants were taken from the compilation by McMasters and Gschneidner[7] as 10.547 and 10.434 Å for Er_2O_3 and Yb_2O_3, respectively.

Tables of observed and calculated structure factors are given in Appendix A. The strongest peaks observed, (222) and (444), were not included in the structure refinement because of extinction. There was also some difficulty at the low end of the intensity scale due to simultaneous reflections, particularly for the relatively large Yb_2O_3 crystal that was used. A very weak reflection can be subject to extremely large fractional intensity changes. For Yb_2O_3 a number of forbidden

[4] R. M. Moon and C. G. Shull, Acta Cryst. **17**, 805 (1964).
[5] M. K. Wilkinson, W. C. Koehler, E. O. Wollan, and J. W. Cable, Bull. Am. Phys. Soc. **2**, 127 (1957); W. C. Koehler, M. K. Wilkinson, E. O. Wollan, and J. W. Cable, Oak Ridge National Laboratory Report No. ORNL-2204, 1956 (unpublished), p. 44.
[6] W. R. Busing, K. O. Martin, and H. A. Levy, Oak Ridge National Laboratory Report No. ORNL-TM-305, 1962 (unpublished).
[7] O. D. McMasters and K. A. Gschneider, Jr., in *International Symposium on Compounds of Interest in Nuclear Reactor Technology, August, 1964* (Edwards Brothers, Ann Arbor, Michigan, 1964), p. 93.

TABLE I. Comparison of structural parameters.

	Er_2O_3		Yb_2O_3		$(Fe, Mn)_2O_3$
	This work	Fert[a]	This work	Fert[a]	Pauling[b]
u[c]	-0.0354 ± 0.0010	-0.0330 ± 0.0006	-0.0321 ± 0.0008	-0.0336 ± 0.0008	-0.030 ± 0.005
x[d]	0.391 ± 0.001	0.394 ± 0.001	0.391 ± 0.001	0.391 ± 0.001	0.385 ± 0.005
y	0.152 ± 0.001	0.149 ± 0.001	0.151 ± 0.001	0.151 ± 0.001	0.145 ± 0.005
z	0.379 ± 0.001	0.380 ± 0.001	0.380 ± 0.001	0.380 ± 0.001	0.380 ± 0.005

[a] A. Fert, Bull. Soc. Franc. Mineral. Crist. **85**, 267 (1962).
[b] Reference 2.
[c] u applies to the C_2 site cation.
[d] x, y, z refer to the oxygen position.

reflections were observed above the magnetic transition, for example the (110) and (310). These were attributed to simultaneous reflections based on measurements obtained on crystals of different sizes. For a weak reflection, including the case of zero structure factor, simultaneous reflections can only increase the observed intensity. In addition, because a double reflection is involved, the spurious intensity will increase faster than linearly with the crystal mass. For two crystals of mass ratio $m_1/m_2>1$, we expect an intensity ratio for equivalent weak reflections of $I_1/I_2>m_1/m_2$ if the intensities are due to simultaneous reflections, and $I_1/I_2=m_1/m_2$ if we are measuring a real single reflection. For Yb_2O_3, decreasing the crystal mass by a factor of 5.5 resulted in an intensity decrease for both the (110) and (310) by a factor of 19. Several other reflections, which should have small but not zero structure factors, also showed abnormally large intensity ratios and were therefore excluded from the structure analysis. Reflections with medium to strong intensities gave intensity ratios roughly equal to the mass ratio. Of course, the simultaneous reflection effects were present in all cases, but they only produced large fractional errors for the weak reflections.

The results of the least-squares analysis are given in Table I together with results of other workers. Perhaps the most interesting aspect of Table I is the good agreement between the recent work on the rare-earth oxides and the original bixbyite structure determination by Pauling and Shappell,[2] in which they arrived at the oxygen parameters by guessing that each oxygen was equidistant from its four neighboring cations.

IV. RESULTS—MAGNETIC STRUCTURES

A. Er_2O_3

Neutron diffraction experiments on powder samples of Er_2O_3 by Koehler *et al.*[5] established the fact that antiferromagnetic ordering occurs at about 4°K. Certain characteristics of the structure were deduced from the occurrence of only those reflections of one even and two odd indices, but a complete structure was not reported. Recent susceptibility measurements by Brown and Hubbard[8] and by Bonrath *et al.*[9] locate the Néel point at 3.4°K.

[8] R. E. Brown and W. M. Hubbard, in Proceedings of the Fifth Rare-Earth Research Conference, 1965 (unpublished), Book 4, p. 31.
[9] H. Bonrath, K. H. Hellwege, K. Nicolay, and G. Weber, Physik Kondensierten Materie **4**, 382 (1966).

Concurrent with the present investigation, work was also underway at Grenoble on the magnetic structure of Er_2O_3. Using group theory to suggest possible structures, Bertaut and Chevalier[10] have proposed a noncollinear antiferromagnetic structure that fits their powder data quite well. Working independently and using quite a different approach to the problem, we arrived at the same structure, differing only slightly in the magnitude of the Er moments. Their success in working out such a complicated structure based on powder diffraction data is a good example of the usefulness of Bertaut's macroscopic theory of spin configurations.[11]

The fact that all the magnetic reflections have $h+k+l=2n$ implies that atoms related by the body center translation have their moments in the same direction. This reduces the number of rare-earth sites with unknown moment directions from 32 to 16. We were led to consider noncollinear structures by the paramagnetic resonance work of Schäfer and Scheller,[12] who found highly anisotropic g tensors for Er^{3+} in Y_2O_3, with the major axis for the C_{3i} sites along the local $\langle 111 \rangle$ symmetry axis and the major axis for the C_2 sites along the local $\langle 100 \rangle$ symmetry axis. By making the following assumptions we arrived at a specific model:

(1) The moment directions are along the local symmetry axis,

(2) the moments on C_{3i} form an antiferromagnetic structure, and

(3) there is an antiferromagnetic Heisenberg interaction between nearest and next-nearest rare-earth ions, resulting from superexchange via the neighboring oxygens.

Assumptions (1) and (2) define a unique configuration for the C_{3i} ions. Using this configuration and assumption (3), the moment directions on the C_2 sites are determined and the resulting configuration is consistent with assumption (1). It was immediately apparent that this model could give agreement with the observed intensities by properly adjusting the magnitude of the moments on the two different sites. This agreement does not imply that the coupling mechanism is necessarily superexchange; we shall see that a classical dipole-

[10] E. F. Bertaut and R. Chevalier, Compt. Rend. **B262**, 1707 (1966).
[11] E. F. Bertaut, in *Magnetism*, edited by G. T. Rado and H. Suhl (Academic Press Inc., New York, 1963), Vol. III, p. 150.
[12] G. Shäfer and S. Scheller, Phys. Kondensierten Materie **5**, 48 (1966).

dipole coupling is also consistent with this model in that the resultant dipole field is along the symmetry axis at each site.

The model generated in this fashion, which is identical to the one proposed by Bertaut and Chevalier,[10] is shown in Fig. 2. The u parameter has been suppressed in this figure; actually all the C_2 sites are displaced along one of the cube edges by about 1/30 of the unit cell. The rare-earth ions may be subdivided into four groups labeled C_{2x}, C_{2y}, C_{2z}, and C_{3i}, where C_{2x} means the eight sites with a twofold axis along [100]. Within each of these groups the ions fall on a simple cubic lattice (when $u=0$) of one-half the full lattice spacing.

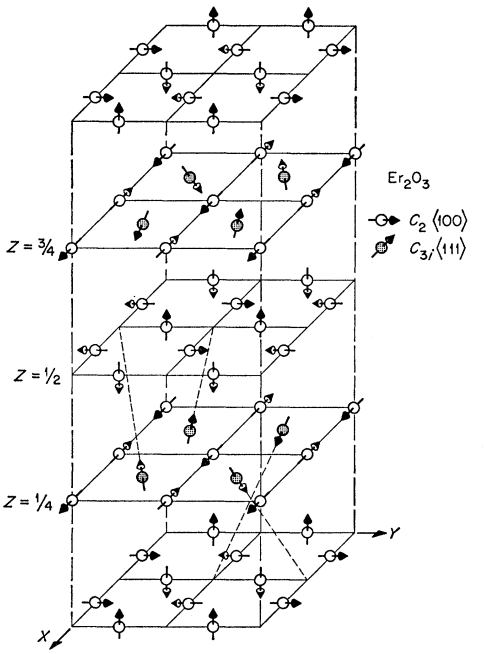

FIG. 2. Magnetic structure of Er_2O_3. The unit cell is cubic but has been expanded along the z direction for clarity. The C_2 sites (open circles) are actually displaced from the positions shown by about 1/30 of a cell edge. The oxygen atoms (not shown) are between the rare-earth layers.

In terms of these sublattices, the magnetic structure is defined in Table II. The $(\pi\pi 0)$ notation means that the moment direction changes through 180° in translating one sublattice unit along x or y and there is no change under a z translation. While the structure seems rather formidable because of the large unit cell and many directions involved, it can be broken down into simple and familiar configurations, as shown in Table II. There are only two magnetic domains, one being formed from the other by reversal of all the moments, and both producing the same neutron scattering. As already noted by Bertaut and Chevalier, the magnetic structure goes into itself under all the operations of the crystallographic space group.

In analyzing the single-crystal data, expressions given in Appendix B were used to calculate structure factors for all the observed magnetic peaks as a function of the moment at the C_2 sites (μ_2) and the ratio (A) of the moment at the C_{3i} site to that at the C_2 site. We have neglected the angular dependence of the moment distribution, which should be different for the two sites, and used the spherical form factors calculated by Blume, Freeman, and Watson.[13] The parameters μ_2 and A were adjusted to minimize the quantity R,

$$R=\sum_i\left(\frac{F_{0i}^2-F_{ci}^2}{\sigma_i}\right)^2\Big/\sum_i\left(\frac{F_{0i}^2}{\sigma_i}\right)^2, \qquad (1)$$

where $F_0^2\pm\sigma$ is the observed square of the structure factor and F_c^2 is the calculated value with the sum going over all the observed peaks. Equivalent reflections were averaged and treated as a single datum. The comparison of observed and calculated structure factors is given in Table III. The best fit was obtained with $\mu_2=(5.08\pm0.19)\mu_B$ and $A=1.11\pm0.05$, giving $R=0.15$.

Powder diffraction results are not subject to the uncertainties of extinction and simultaneous reflections that are very difficult to avoid in single-crystal work, so it is frequently possible to make more accurate absolute

TABLE II. Magnetic sturcture of Er_2O_3.

Sublattice	Component	Magnetic structure
C_{2x}	x	$(\pi\pi 0)$
C_{2y}	y	$(0\pi\pi)$
C_{2z}	z	$(\pi 0\pi)$
C_{3i}	x	$(\pi 0\pi)$
C_{3i}	y	$(\pi\pi 0)$
C_{3i}	z	$(0\pi\pi)$

TABLE III. Observed and calculated magnetic structure factors for Er_2O_3 single crystal.

h	k	l	F_{obs}^2 [a]	F_{calc}^2 [b]	σ
0	1	3	39.5	33.3	1.8
0	3	5	94.6	77.8	4.5
1	1	0	118.2	116.9	3.6
1	1	2	176.3	203.0	6.1
1	2	3	88.1	74.4	4.3
1	2	5	144.6	105.3	9.7
1	3	4	163.8	200.3	10.8
1	4	5	52.2	35.5	10.6
1	5	0	109.2	98.6	4.8
2	3	5	39.5	39.1	6.7
3	2	1	107.2	104.2	5.4
3	3	0	209.0	251.2	6.6
3	3	2	41.9	45.5	11.5
4	1	1	151.0	133.3	6.0
4	3	1	66.5	59.7	6.5
4	3	3	301.1	257.4	11.2
5	1	0	39.7	29.9	3.1
5	2	1	181.5	217.6	8.1
5	3	0	101.4	87.2	5.2
5	4	1	117.3	107.2	8.8
6	1	1	216.4	203.2	11.2

[a] The observed magnetic intensities were put on an absolute basis using a scale factor obtained from the nuclear peaks.

[b] $F_{calc}^2=F^2/f^2$, where F^2 is calculated as in Appendix B.

[13] M. Blume, A. J. Freeman, and R. E. Watson, J. Chem. Phys. 37, 1245 (1962).

TABLE IV. Comparison of observed and calculated magnetic intensities for Er_2O_3 powder.

h	k	l	Observed[a] (arbitrary units)	Calculated
1	1	0	1219±15	1204
2	1	1	4123±58	4182
3	1	0	409±54	371
1	3	0		
3	2	1	3693±120	3694
1	2	3		
3	3	0	5284±122	5333
4	1	1		
3	3	2	997±287	937
4	3	1		
1	3	4	6647±575	6679
5	1	0		
1	5	0		

[a] Observed intensities have been corrected for the Lorentz factor, form factor, Debye-Waller factor, and absorption.

intensity measurements using powder samples. This was true in the case of Er_2O_3. Table IV shows a comparison of observed and calculated intensities using the value of A determined from the single-crystal analysis. The magnetic intensities can be put on an absolute basis by an internal calibration using the nuclear intensities, or by an external calibration using Ni as a standard. Both techniques were employed and gave consistent results. From the powder data, we find $\mu_2=(5.40\pm0.08)\mu_B$. An independent determination of the moment ratio A was obtained by normalizing the observed powder intensities to the observed (110) intensity. This intensity ratio is a function of only one unknown, the parameter A. Each intensity ratio could then be used to determine a value for A. The weighted mean of such values gave $A=1.16\pm0.05$, in satisfactory agreement with the single-crystal determination. Taking a weighted average of the single crystal and powder results, we conclude that $\mu_2=(5.36\pm0.08)\mu_B$ and $\mu_{3i}=(6.06\pm0.32)\mu_B$ at 1.25°K. It is estimated that the moments are 0.5% greater at $T=0$°K. These values are well below the free-ion moment of $9.0\mu_B$.

This result should be compared with that of Bertaut and Chevalier,[10] who found equal moments of $(5.7\pm0.2)\mu_B$ on both sites. The two sets of powder data are in good agreement with each other and the slightly different conclusions can be traced to differences in the methods of analysis. They used a somewhat different u parameter for the C_2 rare-earth site (-0.033 instead of -0.0354). Reanalysis of our data using the smaller u parameter resulted in no change in the moment ratio obtained from the single-crystal data, but shifted this ratio from 1.16 to 1.08 based on the powder data. A second source for the disagreement can be attributed to their method of judging the goodness of fit between calculated and observed intensities. They used an unweighted confidence factor in which the observed intensities had been corrected for the Lorentz factor and the form factor. This has the effect of seriously overestimating the significance of reflections at high angles. Our value for the ratio of the two moments is in good agreement with the unpublished Mössbauer data of Kienle, which was cited by Bertaut and Chevalier.

Some experiments on the influence of a magnetic field were performed on both single crystals and powders. The field effects are very complicated and are not understood. There is evidence for at least two and sometimes three magnetic phases in the presence of a modest applied field.

B. Yb_2O_3

The Néel point of Yb_2O_3 has been established as about 2.4°K by susceptibility[8,9] and magnetization[14] measurements. No previous neutron diffraction work has been reported.

The first step in the present investigation was to obtain a powder diffraction pattern at 1.3°K. Only two magnetic peaks were detected, the (111) and (210). This immediately suggested (because $h+k+l=$odd) that rare-earth sites related by the body-center translation have their moments opposed, in contrast to the Er_2O_3 case, in which they are parallel. After collecting a set of low-temperature single-crystal intensities, various models were considered based on the same type of assumptions which had led us to the Er_2O_3 model.

Paramagnetic resonance experiments by Mandel[15] show a highly anisotropic g tensor for the C_{3i} sites with the major axis along the local symmetry axis, as in the case of Er_2O_3. For the C_2 sites the largest g value is along a [110] direction perpendicular to the twofold axis, in contrast to the Er_2O_3 case, where it is parallel to the rotation axis. We considered models in which the C_{3i} sites had moments along their local symmetry axis, with opposite moments on sites related by the body-center translation. There are eight such configurations, none of which was helpful in generating a satisfactory mode.

An attempt was made to utilize Bertaut's[11] macroscopic theory of spin configurations since this had been helpful to him in working out the Er_2O_3 structure. Combining basis vectors of the same representation in such a way that the C_{3i} moments were along the local symmetry axis did not lead to agreement with the experimental data. However, when this restriction was relaxed, a satisfactory model was found almost immediately.

[14] W. E. Henry, Phys. Rev. **98**, 226 (1955).
[15] M. Mandel. Appl. Phys. Letters **2**, 197 (1963).

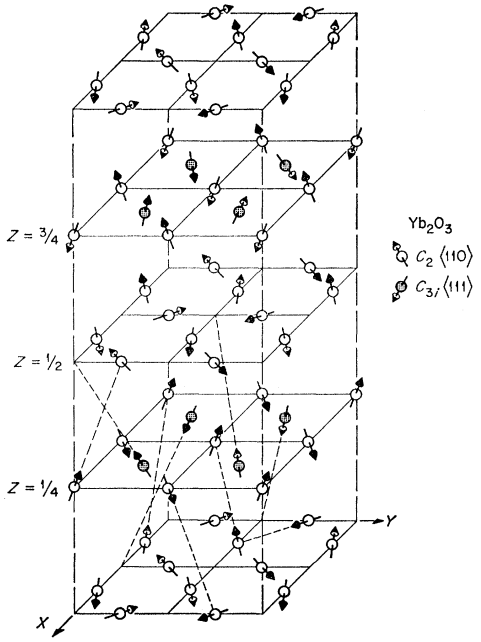

FIG. 3. Magnetic structure of Yb_2O_3. The unit cell is cubic but has been expanded along the z direction for clarity. The C_2 sites (open circles) are actually displaced from the positions shown by about 1/30 of a cell edge. The oxygen atoms (not shown) are between the rare-earth layers.

This is a three-domain model, one of which is shown in Fig. 3. The C_{3i} moments are along [111] directions, but not along the local [111] symmetry axis. The C_2 sites have moments along [110] directions perpendicular to the local twofold axis. In terms of the four sublattices discussed previously, the structure is described in Table V. In the notation of Bertaut and Chevalier,[10] the structure of one of the domains is $g_x-a_y-c_z$ for the C_{3i} sites and $C_{1y}+A_{1z}+C_{2z}-A_{2x}-C_{3x}+A_{3y}$ for the C_2 sites. The second domain is obtained by changing the sign of all x and y components and the third domain obtained by changing the sign of all x and z components.

Magnetic structure factors were calculated as outlined in Appendix B. These are compared with experimental values in Table VI. The best least-squares fit with the single-crystal data was obtained for $\mu_2=(1.81\pm0.08)\mu_B$ and $A=0.565\pm0.024$, giving $R=0.14$. From the two powder peaks we obtained $\mu_2=(1.91\pm$

TABLE V. Magnetic structure of Yb_2O_3.

Sublattice	Component	Magnetic structure
C_{2x}	y	(00π)
C_{2x}	z	$(\pi\pi\pi)$
C_{2y}	z	$(\pi00)$
C_{2y}	x	$(\pi\pi\pi)$
C_{2z}	x	$(0\pi0)$
C_{2z}	y	$(\pi\pi\pi)$
C_{3i}	x	$(0\pi0)$
C_{3i}	y	(00π)
C_{3i}	z	$(\pi00)$

TABLE VI. Observed and calculated magnetic structure factors for Yb_2O_3 single crystal.

h	k	l	F_{obs}[2a]	F_{calc}[2b]	σ
0	2	5	27.85	33.75	1.19
0	3	0	8.35	9.40	0.29
0	5	2	2.97	2.19	0.19
1	0	0	1.02	0.88	0.04
1	1	1	21.52	19.62	0.33
1	2	0	10.71	10.69	0.37
1	4	0	0.37	0.01	0.16
1	5	3	6.23	7.39	0.85
1	6	0	3.21	2.89	0.34
2	1	0	3.13	3.84	0.15
2	2	1	3.37	3.19	0.17
2	3	0	7.49	5.42	0.32
3	1	1	9.67	10.65	0.36
3	2	0	27.50	29.15	0.90
3	2	2	0.69	0.70	0.28
3	3	3	14.08	13.83	0.63
3	4	2	4.48	3.31	0.25
4	1	0	3.33	3.52	0.33
4	3	2	10.11	12.84	1.43
4	4	1	4.10	3.87	0.32
4	4	3	5.18	6.97	0.37
5	1	1	12.03	11.23	0.56
5	1	3	7.46	8.01	0.55

[a] The observed magnetic intensities were put on an absolute basis using scale factor obtained from the nuclear peaks.

[b] $F_{calc}^2=F^2/f^2$, where F^2 is calculated as in Appendix B.

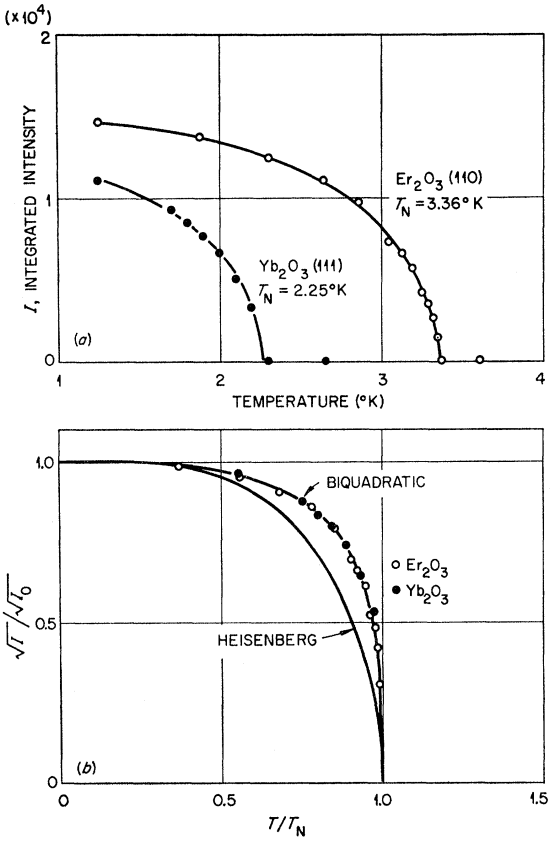

FIG. 4. Temperature dependence of magnetic reflections of Er_2O_3 and Yb_2O_3. The solid curves in (b) are calculated molecular-field approximations for the Heisenberg and biquadratic exchange interactions.

$0.08)\mu_B$ and $A=0.54\pm0.19$. The weighted average gives $\mu_2=(1.86\pm0.06)\mu_B$ and $\mu_{3i}=(1.05\pm0.06)\mu_B$ at 1.25°K. It is estimated that these values are 2% below the saturation moment at 0°K. The free-ion moment is $4.0\mu_B$.

C. Temperature Dependence of Long-Range Order

The temperature dependences of the (111) reflection in Yb_2O_3 and the (110) reflection in Er_2O_3 are shown in Fig. 4(a). The indicated Néel points are in good agreement with susceptibility data.[8,9] The normalized square root of these data, which is proportional to the average ordered moment, is plotted as a function of reduced temperature in Fig. 4(b). It is apparent that the reduced temperature dependence is the same in both cases.

For both systems the crystal-field ground state is a doublet and the first excited state has an energy large compared to kT_N. If a molecular field approximation is valid, one would expect the temperature dependence to follow the $S=\frac{1}{2}$ Brillouin-Weiss function

$$\sigma=\tanh(\mu_0 H_e/kT), \tag{2}$$

where μ_0 is the moment at $T=0$ and $\sigma=\mu/\mu_0$. In the molecular field approximation to the Heisenberg interaction, we have

$$H_e=\lambda\sigma. \tag{3}$$

Using the condition at the Néel point to define λ, Eq. (2) may be written as

$$\sigma=\tanh(\sigma/\tau), \tag{4}$$

where $\tau=T/T_N$. This function, labeled "Heisenberg" in Fig. 4(b), is not in agreement with the observations. This is not surprising, because Elliott and Thorpe[16] have shown that for systems in which orbital contributions to the magnetic moment are important, the exchange interaction is not of the Heisenberg form.

The shape of the observed temperature variation suggested that a biquadratic exchange term might be important. We assume a molecular-field approximation of the form

$$H_e=\lambda\sigma(1+\beta\sigma^2). \tag{5}$$

The parameter λ may be eliminated as before, and Eq. (2) may be written as

$$\sigma=\tanh[\sigma(1+\beta\sigma^2)/\tau]. \tag{6}$$

A value of $\beta=0.273$ was used in calculating the curve in Fig. 4(b). While the agreement with the data is very striking, we do not regard this as convincing proof of the importance of biquadratic exchange. Aside from the question of a proper theoretical basis for Eq. (6), there is the possibility of unusual temperature effects in Er_2O_3 due to admixtures of higher crystal-field levels.

[16] R. J. Elliott and M. F. Thorpe, J. Appl. Phys. **39**, 802 (1968).

V. DISCUSSION OF RESULTS

A. Dipole-Dipole Interactions

A computer program was written to perform a lattice sum of the classical dipole-dipole interaction. The field at each site was calculated by summing contributions from the other sites,

$$\mathbf{H}(r_i)=-\sum_{j\neq i}\left(\frac{\boldsymbol{\mu}_j}{r_{ij}^3}-\frac{3(\boldsymbol{\mu}_j\cdot\mathbf{r}_{ij})\mathbf{r}_{ij}}{r_{ij}^5}\right), \tag{7}$$

where $\mathbf{r}_{ij}=\mathbf{r}_j-\mathbf{r}_i$ and the energy of the moment at site i is then $E_i=-\boldsymbol{\mu}_i\cdot\mathbf{H}(r_i)$. The convergence of this summation was investigated by including all sites within a sphere of radius R_M and ignoring ions outside this sphere. The results for the C_2 site in Er_2O_3 are shown in Table VII as a function of R_M. On the basis of these results it was concluded that satisfactory numbers could be obtained by terminating the calculation at $R_M=2.0$ lattice units (about 21 Å).

Results of the field and energy calculations for various sites in Er_2O_3 are shown in Table VIII. The structure is consistent with a dipole-dipole interaction as the dominant coupling mechanism in that the field at each site is in the direction of the moment at that site. Further, the interaction energy at the C_{3i} site is comparable to the observed Néel temperature of 3.4°K. However, the energy of the C_2 moments is an order of magnitude lower and the average energy[17] is 1.26°K, too low to give a satisfactory explanation of the observed Néel point. We conclude that the dipole-dipole interaction is not the dominant coupling mechanism, but neither is it negligible for Er_2O_3.

For Yb_2O_3, the same calculation gives no hope of explaining the results in terms of the dipole-dipole interaction. The field at each site is not in the direction of the moment at that site and the average energy is 0.017°K.

B. Crystal-Field Effects

The key to understanding the complexity and diversity of the magnetic structures of the rare-earth

TABLE VII. Convergence of dipole sum.

R_M lattice units	No. of ions within R_M	$E(C_2)$ °K
1.0	140	3.59
1.5	446	3.97
2.0	1057	3.92
3.0	3624	3.91
4.0	8543	3.90

[17] The contribution per atom to the energy of the system is $\frac{1}{2}$ this average energy.

TABLE VIII. Dipole energy at various sites in Er_2O_3.

Type	Position x	y	z	Moment (μJ) μ_x	μ_y	μ_z	Field (kg) H_x	H_y	H_z	Energy (°K)
C_{3i}	0.25	0.25	0.25	3.5	3.5	3.5	5.6	5.6	5.6	−3.92
C_{3i}	0.25	0.75	0.75	−3.5	−3.5	3.5	−5.6	−5.6	5.6	−3.92
C_2	0.965	0	0.25	5.4	0	0	1.0	0	0	−0.38
C_2	0.465	0	0.25	−5.4	0	0	−1.0	0	0	−0.38
C_2	0.25	0.965	0	0	5.4	0	0	1.0	0	−0.38

oxides probably lies in the angular part of the wave functions of the crystal-field ground state. Unfortunately, our knowledge of the wave functions is very incomplete.

In the case of the C_2 sites in Er_2O_3 there was hope that some basic understanding could be reached. Optical measurements by Gruber *et al.*[18] and by Rosenberger[19] have established the energy splittings of the free-ion ground-state multiplet by the crystal field. There are eight doublets with the first excited state about 56°K above the ground state and an over-all splitting of 733°K. Eicher[20] has analyzed Rosenberger's data and published a ground-state wave function. Gruber *et al.*[21] have given wave functions for all eight doublets. Unfortunately, the two ground-state wave functions are not in agreement with each other. Based on Eicher's function, we calculate $\langle\psi_0 \mid J_z \mid \psi_0\rangle = 0.0029$, and using the Gruber function, $\langle\psi_0 \mid J_z \mid \psi_0\rangle = -1.769$. The Gruber wave functions should be more reliable because they were obtained by fitting a much larger number of energy levels and because Eicher made a questionable assumption in simplifying the symmetry from C_2 to C_{2v}. The problem of obtaining the proper wave functions from observed energy levels is very difficult because it involves the determination of 14 crystal-field parameters.

For the moment, let us accept the Gruber wave functions and attempt to relate them to our measurements. The z axis for the wave functions is the twofold symmetry axis that is also the direction of the ordered moments for the C_2 sites in Er_2O_3. In a relatively weak effective field along the symmetry axis, we would expect an ordered moment at 0°K of $g_L\langle\psi_0 \mid J_z \mid \psi_0 = 2.12\mu_B$, whereas we observe $5.36\mu_B$. This is not a serious disagreement because a stronger effective field will result in a new ground state formed by mixing the crystal-field states[1] and the moment can be easily increased. In fact, an effective field of about 65 kOe will produce the observed moment. The ordered moment is thus not a very good check on the validity of crystal-field wave functions.

To justify an analysis of our results in terms of these wave functions it seemed important to have a check on their validity. Accordingly, calculations of susceptibility and the g tensor were performed and compared with available experimental data.

The powder susceptibility data of Hacker *et al.*[22] showed a linear $1/\chi$-versus-T relationship down to 10°K with a slope characteristic of the Er^{3+} free ion. It seemed unlikely that the energy levels and wave functions given by Gruber *et al.*[21] would result in such behavior because the total crystal-field splitting was over 700°K. However, the calculation was in remarkable agreement with experiment, giving a linear $1/\chi$ function down to 10°K with an effective moment for the C_2 sites of $9.61\mu_B$. The free-ion effective moment is $9.58\mu_B$. The main conclusion is that powder susceptibility is very insensitive to crystal-field effects and is a poor check on the validity of the wave functions under consideration.

The g factor calculation for a Kramers doublet (ψ_0 and ψ_0') involves the energy splitting in response to a magnetic field of arbitrary direction. We obtain

$$\Delta E = g\mu_B H = 2g_L\mu_B(H_z^2 \mid \langle\psi_0 \mid J_z \mid \psi_0\rangle \mid^2 + \mid H_x\langle\psi_0' \mid J_x \mid \psi_0\rangle + H_y\langle\psi_0' \mid J_y \mid \psi_0\rangle \mid^2)^{1/2}, \quad (8)$$

where g is the experimental g factor along $\mathbf{H}$ and g_L is the Landé g factor. The matrix elements are readily calculated from the Gruber ground state and comparison may then be made with experimental paramagnetic resonance results. The only difficulty is in relating the coordinate system of the calculation to the experimentally determined axes. There is no ambiguity about the z direction; this is the local C_2 symmetry axis for both the wave functions and the resonance results. To

[18] J. B. Gruber, J. R. Henderson, M. Muramoto, K. Rajnak, and J. G. Conway, J. Chem. Phys. **45**, 477 (1966); P. Kisliuk, W. F. Krupke, and J. B. Gruber, *ibid.* **40**, 3606 (1964).
[19] D. Rosenberger, Z. Physik **167**, 360 (1962).
[20] H. Eicher, Z. Physik **169**, 178 (1962).
[21] J. B. Gruber, W. F. Krupke, and J. M. Poindexter, J. Chem. Phys. **41**, 3363 (1964).
[22] H. Hacker, Jr., M. S. Lin, and E. F. Westrum, Jr., in *Proceedings of the Fourth Conference on Rare-Earth Research*, edited by LeRoy Eyring (Gordon and Breach, Science Publishers, Inc., New York, 1965).

TABLE IX. Observed and calculated nuclear-structure factors for Er_2O_3 at 4.2°K.

h	k	l	F_{obs}^2	F_{calc}^2	σ
0	2	0	1.8	1.6	0.2
0	4	0	5.2	3.8	0.4
1	1	$\bar{2}$	19.0	20.2	0.8
1	2	3	12.9	10.8	1.0
1	3	4	62.8	50.4	3.5
1	2	5	34.5	32.8	2.2
1	2	7	124.7	111.1	6.2
1	3	6	115.9	108.3	4.2
1	4	5	75.9	72.2	3.2
2	3	5	28.6	26.1	2.0
2	3	7	144.3	126.7	5.7
$\bar{2}$	3	7	137.2	126.7	4.4
3	2	1	29.9	23.5	1.6
3	3	2	137.2	167.6	4.8
$\bar{3}$	4	5	2.6	0.2	0.6
3	6	7	167.2	167.2	6.3
3	7	2	135.9	126.7	5.2
4	1	1	8.8	9.1	1.1
4	3	1	30.8	26.7	2.3
$\bar{4}$	3	1	32.8	26.7	3.1
4	3	3	15.0	16.5	1.6
5	2	1	26.3	23.3	1.0
5	3	2	36.1	34.9	2.1
5	4	1	31.6	29.8	2.0
$\bar{5}$	4	3	29.6	28.1	2.8
6	1	1	41.8	41.2	2.5
6	2	2	315.0	338.1	9.9
6	3	1	80.9	89.2	3.3
6	6	2	250.1	225.4	9.9
7	2	1	190.6	240.9	6.9
7	2	3	142.2	126.7	5.5
$\bar{7}$	2	3	120.3	126.7	4.6
7	$\bar{3}$	2	57.1	55.5	3.2
7	3	2	61.3	55 5	3.4
7	6	3	239.5	255.4	8.5
8	4	4	602.7	614.7	18.8

obtain g_z, we set $H_x=H_y=0$ in Eq. (8). To obtain g_x and g_y, we set $H_z=0$, $H_x=H\cos\phi$, $H_y=H\sin\phi$, and look for extrema in ΔE as a function of ϕ. In this manner we obtain $g_z=4.25$, $g_x=12.05$, and $g_y=0.40$. These numbers are to be compared with the resonance results of Schäfer and Scheller,[12] who found $g_z=12.314$, $g_x=1.645$, and $g_y=4.892$. There is no good reason to question the resonance results, so we are forced to conclude that the Gruber wave functions are wrong.

C. Superexchange Considerations

Basic understanding of the possible superexchange interactions must await the determination of accurate wave functions. However, it seems worthwhile to examine the geometry involved in the rare-earth oxygen rare-earth interaction.

If the u parameter (C_2 site) were zero, each rare earth would have 12 nearest rare-earth neighbors, four from each of the other three sublattices mentioned previously. With $u=-0.035$ this group of 12 is split into six neighbors at about 3.49 Å and six at about 4.00 Å. Since the rare-earth-oxygen distance is almost 2.28 Å in all cases, we have bond angles of about 100° for nearest neighbors and 125° for the next-nearest. The larger bond angle would favor the next-nearest-neighbor interaction.

As mentioned previously, we were led to the Er_2O_3 structure by assuming an antiferromagnetic superexchange interaction. However, it seems pointless to pursue this model further at the present time, because it was not particularly helpful in the Yb_2O_3 case and because the temperature dependence indicates that the Heisenberg-type interaction may be wrong.

We conclude that something in addition to dipole-dipole forces is necessary to explain these magnetic structures. The temperature dependence of the long-range magnetic order suggests that the interaction may have a biquadratic form. The determination of accurate crystal-field wave functions is a necessary first step toward understanding these structures on a more fundamental level.

Note added in proof. In a recent letter to us, Bertaut has suggested an alternate model for the Yb_2O_3 magnetic structure. In his notation,[10] the structure is described by the following component modes for the C_{3i} sites:

$$g_x=(\tfrac{2}{3})^{1/2}\mu_{3i}\cos\psi,$$

$$a_y=(\tfrac{2}{3})^{1/2}\mu_{3i}\cos(\psi-\tfrac{1}{3}2\pi),$$

$$c_z=(\tfrac{2}{3})^{1/2}\mu_{3i}\cos(\psi+\tfrac{1}{3}2\pi),$$

TABLE X. Observed and calculated nuclear-structure factors for Yb_2O_3 at 4.2°K.

h	k	l	F_{obs}^2	F_{calc}^2	σ
0	2	6	57.0	54.2	1.8
0	4	0	128.2	153.6	3.9
1	2	3	6.9	3.6	0.3
1	4	5	125.4	121.8	3.8
1	4	7	53.8	54.1	1.7
2	1	1	33.4	34.2	1.0
2	3	5	39.4	38.8	1.3
2	3	7	104.5	102.7	3.2
$\bar{2}$	3	7	100.7	102.7	3.1
3	2	1	18.7	13.0	0.6
3	5	6	69.5	68.3	2.2
4	1	1	26.1	28.5	0.8
4	3	3	41.2	42.4	1.3
4	4	4	112.9	117.4	3.4
5	3	2	52.4	53.6	1.7
5	4	1	69.2	66.1	2.2
5	5	4	21.2	21.6	0.8
6	1	1	86.8	92.0	2.7
6	2	0	18.0	15.3	0.6
6	5	3	71.1	68.8	2.2
$\bar{7}$	2	3	97.8	102.8	3.0
7	3	2	35.5	38.1	1.2
7	4	1	29.0	26.6	1.0

and for the C_2 sites,

$$A_{1z}=\mu_2\cos\phi, \qquad C_{1y}=\pm\mu_2\sin\phi,$$

$$A_{2x}=\mu_2\cos(\phi-\tfrac{1}{3}2\pi), \qquad C_{2z}=\pm\mu_2\sin(\phi-\tfrac{1}{3}2\pi),$$

$$A_{3y}=\mu_2\cos(\phi+\tfrac{1}{3}2\pi), \qquad C_{3x}=\pm\mu_2\sin(\phi+\tfrac{1}{3}2\pi).$$

This model involves the same component modes as our model, but in this model all the moments are perpendicular to the local symmetry axis. We have used a three-domain configuration to compare this model with our observations. The second domain is obtained from the above equations by adding $\frac{1}{3}2\pi$ to ψ and ϕ, and the third domain is obtained by subtracting $\frac{1}{3}2\pi$ from ψ and ϕ. The total intensity then becomes a function of $(\psi-\phi)$ and not of the two angles individually. We find that this three-domain model based on Bertaut's proposal fits the data somewhat better than our model, which is not too surprising because the models are similar yet his has an extra parameter to adjust. We find that $R=0.11$ with $\mu_{3i}=1.06\pm0.06\mu_B$, $\mu_2=1.77\pm0.08\mu_B$, $(\psi-\phi)=38°$, and the negative sign taken for the C modes. Note that the moments obtained from either model are nearly identical. The dipole energy calculation indicates that neither model is consistent with dipole-dipole coupling. Neither model is consistent with the resonance results of Mandel[15] concerning the direction of the moments on the C_{3i} sites, while our model is consistent with the resonance results for the C_2 sites. With the present information, there seems to be no clear choice between these two models.

ACKNOWLEDGMENTS

We are indebted to K. H. Hellwege for the single crystals of Er_2O_3 and Yb_2O_3, and to H. L. Davis for many informative discussions on crystal-field effects.

APPENDIX A

Tables IX and X give the comparison of observed and calculated F^2 values for the nuclear peaks observed at 4.2°K. In the final least-squares refinement, the variables were the four-position parameters, the scale factor, and a single isotropic temperature factor. The temperature factor is contained in the calculated structure factors. For both the Er_2O_3 and Yb_2O_3 cases the weighted confidence factor [given by Eq. (1)] was 0.12.

APPENDIX B

The general expression for the magnetic structure factor is

$$\mathbf{F}=\sum p_i\mathbf{q}_i\exp(i\mathbf{k}\cdot\mathbf{r}_i), \tag{B1}$$

where

$$\mathbf{q}_i=\hat{k}(\hat{k}\cdot\hat{\mu}_i)-\hat{\mu}_i, \tag{B2}$$

and $\hat{\mu}_i$ is a unit vector in the moment direction at site i. In dealing with noncollinear structures it is convenient to express the moment directions in terms of their components $C_{\alpha i}$ along the cube edges, where

$$\hat{\mu}_i=\sum_\alpha C_{\alpha i}\hat{x}_\alpha. \tag{B3}$$

If we define

$$\mathbf{q}_\alpha=\hat{k}(\hat{k}\cdot\hat{x}_\alpha)-\hat{x}_\alpha, \tag{B4}$$

we find that

$$\mathbf{F}=\sum_\alpha \mathbf{q}_\alpha G_\alpha, \tag{B5}$$

where

$$G_\alpha=\sum_i p_i C_{\alpha i}\exp(i\mathbf{k}\cdot\mathbf{r}_i). \tag{B6}$$

The quantities G_α are structure factors obtained by decomposing the structure into three orthogonal collinear structures and are combined according to Eq. (B5) to get the total structure factor. Note that the $\mathbf{q}_\alpha$ are not orthogonal except in special cases. The observed intensities are proportional to

$$\mathbf{F}\cdot\mathbf{F}^*=\sum_\alpha\sum_\beta \mathbf{q}_\alpha\cdot\mathbf{q}_\beta G_\alpha G_\beta^*. \tag{B7}$$

For Er_2O_3 the G_α are given by

$$G_x=2p[2(1-\cos\pi h)\cos2\pi(hu+\tfrac{1}{4}l)$$
$$+\tfrac{1}{3}\sqrt{3}A(-1)^n(1-\cos\pi h+\cos\pi k-\cos\pi l)], \tag{B8}$$

where $h+k+l=2n$ and A is the ratio of the moment at the C_{3i} sites to that at the C_2 sites. The magnetic scattering amplitude p is given by

$$p=0.27f\mu_2\times10^{-12}\text{ cm}, \tag{B9}$$

where f is the form factor. Similar expressions can be written for G_y and G_z by permuting the indices in Eq. (B8).

For the Yb_2O_3 model, we find

$$G_x=2ip[-\sqrt{2}(1-\cos\pi k)\sin2\pi(ku+\tfrac{1}{4}h)$$
$$-\sqrt{2}(1+\cos\pi l)\sin2\pi(lu+\tfrac{1}{4}k)$$
$$+\tfrac{1}{3}\sqrt{3}A(-1)^n(1+\cos\pi h-\cos\pi k+\cos\pi l)], \tag{B10}$$

where $h+k+l=2n+1$. To obtain G_y, permute the indices and change the sign, and permute once more to obtain G_z.